NMR spectroscopy | Hot Paper

DOI: 10.1002/anie.201405976

Visualizing an Ultra-Weak Protein–Protein Interaction in Phosphorylation Signaling**

Qiong Xing, Peng Huang, Ju Yang, Jian-Qiang Sun, Zhou Gong, Xu Dong, Da-Chuan Guo, Shao-Min Chen, Yu-Hong Yang, Yan Wang, Ming-Hui Yang, Ming Yi, Yi-Ming Ding, Mai-Li Liu, Wei-Ping Zhang, and Chun Tang**

Abstract: *Proteins interact with each other to fulfill their functions. The importance of weak protein–protein interactions has been increasingly recognized. However, owing to technical difficulties, ultra-weak interactions remain to be characterized. Phosphorylation can take place via a $K_D \approx 25$ mM interaction between two bacterial enzymes. Using paramagnetic NMR spectroscopy and with the introduction of a novel Gd^{III}-based probe, we determined the structure of the resulting complex to atomic resolution. The structure accounts for the mechanism of phosphoryl transfer between the two enzymes and demonstrates the physical basis for their ultra-weak interaction. Further, molecular dynamics (MD) simulations suggest that the complex has a lifetime in the micro- to millisecond regimen. Hence such interaction is termed a fleeting interaction. From mathematical modeling, we propose that an ultra-weak fleeting interaction enables rapid flux of phosphoryl signal, providing a high effective protein concentration.*

A protein interacts with its partner proteins to fulfill its functions and to establish its identity in cell. Though tens of thousands of protein–protein interactions have been predicted,[1] many of the interactions have never been experimentally validated. This can be due to that the interactions are too weak to be visualized with standard techniques.[2] Indeed, among the thousands of atomic resolution structures determined for protein–protein complexes, most of them are tightly bound with the binding affinity K_D values below 1 μM, and only a small fraction is in the weak-binding regimen with the K_D above 1 μM.[3] Notwithstanding, weak protein–protein interactions are involved in cell signaling and many important cellular processes. How proteins weakly interact is of great biological and chemical interest.[4]

Among the techniques to visualize protein–protein interactions, nuclear magnetic resonance (NMR) spectroscopy is particularly suited to weak ones. Protein–protein complexes with K_D values up to a few millimolar can be determined by using solution NMR spectroscopy on the basis of intermolecular nuclear Overhauser effect (NOE).[4–5] But the questions are whether even weaker interactions—with K_D values in the tens of millimolar—exist and can be detected and characterized, and whether these ultra-weak interactions are functionally relevant. To address these questions, however, calls for more sensitive biophysical and NMR techniques.

Phosphorylation is an important cell signaling mechanism that employs a phosphoryl group as the token of signal.[6] Phosphotransferase system (PTS) is a two-component signaling network in bacteria, responsible for sensing and using a certain nutrient.[7] In the PTS, enzyme I (EI) is first autophosphorylated,[8] and then transfers the phosphoryl group to enzyme IIA-Glucose ($EIIA^{Glc}$) via enzyme histidine phosphorcarrier (HPr).[9] As an alternative pathway, we found that, $EIIA^{Glc}$ can be phosphorylated by EI in the absence of HPr, at the same active-site residue H90 based on these evidences.

The NMR spectra of the phosphorylated $EIIA^{Glc}$ (p-$EIIA^{Glc}$) are identical either in the presence or absence of HPr (Figure 1a and Figure S1 in the Supporting Information). From the increase in peak intensities for *p*-$EIIA^{Glc}$ and the simultaneous decrease in peak intensities for the unphosphorylated $EIIA^{Glc}$, we were able to monitor the progress of $EIIA^{Glc}$ phosphorylation (Figure 1b). Addition of an HPr active-site[10] mutant, HPr-H15 A, obstructs the direct phosphorylation of $EIIA^{Glc}$ by EI, in a dose-dependent manner (Figure 1c), as the mutant competes for the same interfaces and forms non-productive complexes. The direct phosphoryl transfer from EI to $EIIA^{Glc}$ was also confirmed in vivo. With the gene-encoding HPr protein, *ptsH*, knocked out from the *E. coli* genome, the resulting Δ*ptsH* strain was still able to grow on the minimum medium and consume glucose, albeit at a slower rate (Figure 1d). With the HPr-H15A mutant gene

[*] P. Huang,[+] Prof. W.-P. Zhang[+]
Department of Pharmacology and Institute of Neuroscience
Zhejiang University School of Medicine
Yu-Hang-Tang Road, Hangzhou, Zhejiang 310028 (China)
E-mail: weiping601@zju.edu.cn
Q. Xing,[+] J. Yang, J.-Q. Sun, Dr. Z. Gong, Dr. X. Dong, Dr. D.-C. Guo, S.-M. Chen, Y.-H. Yang, Y. Wang, Prof. M.-H. Yang, Dr. M. Yi, Prof. Y.-M. Ding, Prof. M.-L. Liu, Prof. C. Tang
CAS Key Laboratory of Magnetic Resonance in Biological Systems
Wuhan Center for Magnetic Resonance
State Key Laboratory of Magnetic Resonance and Atomic Molecular Physics, Wuhan Institute of Physics and Mathematics of the Chinese Academy of Sciences
Xiao-Hong Shan, Wuhan, Hubei 430071 (China)
E-mail: tanglab@wipm.ac.cn
Homepage: http://tanglab.wipm.ac.cn
[+] These authors contributed equally to this work.

[**] We thank the Chinese Ministry of Science and Technology (grant number 2013CB910200) and the National Natural Sciences Foundation of China (grant numbers 31225007 and 31170728) for support. C.T. was supported in part by an International Early Career Scientist grant from the Howard Hughes Medical Institute. The coordinates for the EIN-$EIIA^{Glc}$ complex at 2% occupancy together with experimental restraints are deposited in the PDB with the accession code 2MP0.

Supporting information for this article is available on the WWW under http://dx.doi.org/10.1002/anie.201405976.

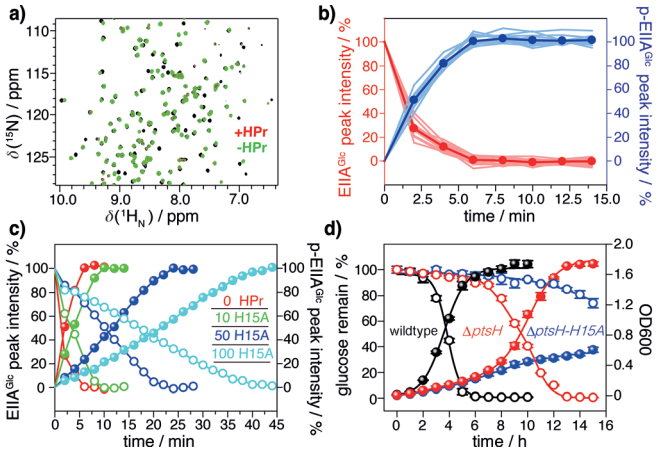

Figure 1. Phosphorylation of EIIA^{Glc} by enzyme EI. a) Overlay of 2D ^{1}H–^{15}N correlation spectra for the unphosphorylated EIIA^{Glc} (black) and phosphorylated EIIA^{Glc} either through HPr (red) or by EI directly (green). Note that the green spectrum is right on top of the red one. b) Time course of EIIA^{Glc} phosphorylation. Each light trace represents the change in relative peak intensity for a residue during phosphorylation. The averaged ratios are shown as filled circles and are connected by a solid line. c) EIIA^{Glc} phosphorylation (300 μM) by a catalytic amount of EI (0.3 μM) is obstructed by the increasing amount of HPr active-site mutant HPr-H15A (0, 3, 15, 30 μM for red, green, blue, and cyan lines, respectively). d) Growth curves (measured by OD600) and glucose consumption are compared between the wild-type, Δ*ptsH* and Δ*ptsH*-H15A strains. The Δ*ptsH* strain is obtained by knocking out the gene encoding HPr protein, *ptsH*, from the *E. coli* genome; the Δ*ptsH*-H15A strain is obtained by knocking back the HPr-H15A mutant gene.

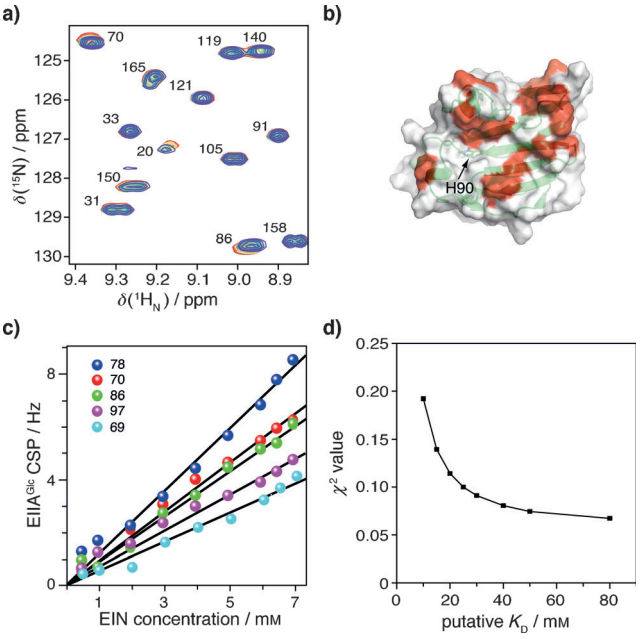

Figure 2. NMR titration of EIIA^{Glc} with EIN. a) Overlay of a region of 2D ^{1}H–^{15}N correlation spectra of EIIA^{Glc} titrated with EIN up to 7 mM. The spectral resolutions in $^{1}H_N$ and ^{15}N dimensions are 4.695 Hz/point and 7.128 Hz/point, respectively. b) Residues with chemical shift perturbations (CSPs) > 3 Hz are mapped onto the surface of EIIA^{Glc}. c) EIIA^{Glc} CSPs are plotted against the concentrations of EIN. d) EIIA^{Glc} CSPs are fitted to theoretical binding isotherms with putative K_D values. The residual χ^2 values from the fitting are plotted against the K_D.

knocked back in, the Δ*ptsH*-H15A strain was found to grow more slowly with slower glucose consumption than the Δ*ptsH* strain (Figure 1d). Taken together, enzyme EI phosphorylates EIIA^{Glc} directly. In doing so, enzyme EI, especially its N-terminal domain (EIN) where the active-site residue H189 is located,[8] has to directly interact with EIIA^{Glc}.

The binding affinity between EI and EIIA^{Glc}, however, turned out to be extremely weak. We performed NMR titration with the unlabeled EIN, up to 7 mM, into the ^{15}N-labeled EIIA^{Glc}. The resulted chemical shift perturbations (CSPs) for EIIA^{Glc} are smaller than 9 Hz or about 0.01 ppm on an 800 MHz NMR spectrometer (Figure 2a). Titration of the full-length EI, up to 4 mM, into EIIA^{Glc} gives even smaller CSPs for EIIA^{Glc} (Figure S2). Though most of the perturbed residues form a somewhat contiguous surface and can be mapped to the vicinity of EIIA^{Glc} active-site residue H90 (Figure 2b), plotting EIIA^{Glc} CSPs against EIN protein concentration yields almost straight lines (Figure 2c). A plausible fit for the CSPs can only be obtained with a K_D value larger than 20 mM, as the residual χ^2 value begins to level off (Figure 2d and Figure S3). Inverse titration of unlabeled EIIA^{Glc} into U-[^{2}H,^{15}N]-labeled EIN affords even smaller CSPs (Figure S4). The small CSPs result from the extremely low occupancy of the EIN-EIIA^{Glc} complex at the concentrations permitted by protein solubility. As the standard NMR approach requires a significant population of the protein in the complexed form,[4] it would not be feasible to characterize the structure of the EIN-EIIA^{Glc} complex based on intermolecular NOEs.

Thus we resorted to paramagnetic NMR spectroscopy.[11] We were only able to obtain intermolecular restraints using a Gd^{3+}-based paramagnetic probe; Gd^{3+}-EDTA-benzyl-acetate (Figure S5) was conjugated at an engineered cysteine in either EIN or EIIA^{Glc}, and the paramagnetic relaxation enhancement (PRE) rates were assessed for the ^{15}N-labeled partner protein. Gd^{3+} is a lanthanide ion with a large spin quantum number ($S = 7/2$) and long electron relaxation time ($\tau_e \approx 10$ ns).[12] At a given electron–proton distance, Gd^{3+} causes the PRE effect twice as large as transition metal Mn^{2+} and ten times as large as nitroxide radical. Despite of the more favorable relaxation property of Gd^{3+}, intermolecular PREs for some of the conjugation sites (Q87C, S113C, and E117C on EIN) are still smaller than 5 s^{-1}. The largest intermolecular PREs were afforded for EIIA^{Glc} with the probe conjugated at the EIN E63C site, and for EIN with the probe conjugated at the EIIA^{Glc} E43C site (Figure 3). Even for these two sites, no residue was completely broadened out or has a PRE value > 80 s^{-1}.

To determine the complex structure, we performed rigid-body simulated annealing, by refining against the intermolecular PRE restraints for EIN E63C, EIN E117C, and EIIA^{Glc} E43C sites. The occupancy of the complex was varied from 0.1 to 5%. The best agreement between the observed and back-calculated Gd^{3+} PREs was achieved with the complex formed at 2–5% of the time, while occupancy of 1% or less resulted in large van der Waals repulsive energy and large PRE Q-factor (Figure 4a). At the protein concentrations employed for the PRE experiments, a 2% occupancy

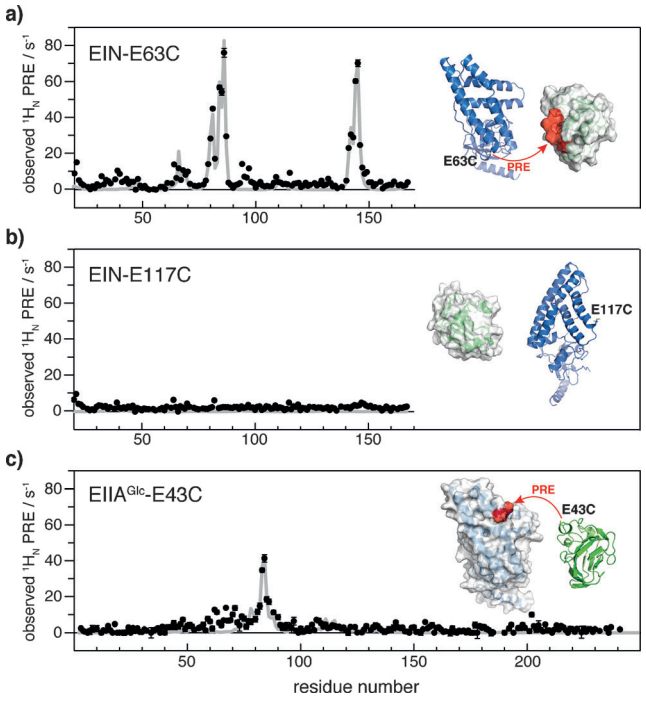

Figure 3. Intermolecular PREs between EIN and EIIA^{Glc}. Using a Gd^{3+}-based paramagnetic probe, the PRE values were measured for a) EIIA^{Glc} at EIN E63C, b) for EIIA^{Glc} at E117C sites, and c) for EIN at EIIA^{Glc} E43C site. Observed PREs are shown as black dots, error bar representing 1 standard deviation. The back-calculated PREs are shown as grey lines. Insets show the structures of individual proteins, with the cysteine conjugation sites and residues with large PREs ($\Gamma_2 > 20\ s^{-1}$) illustrated.

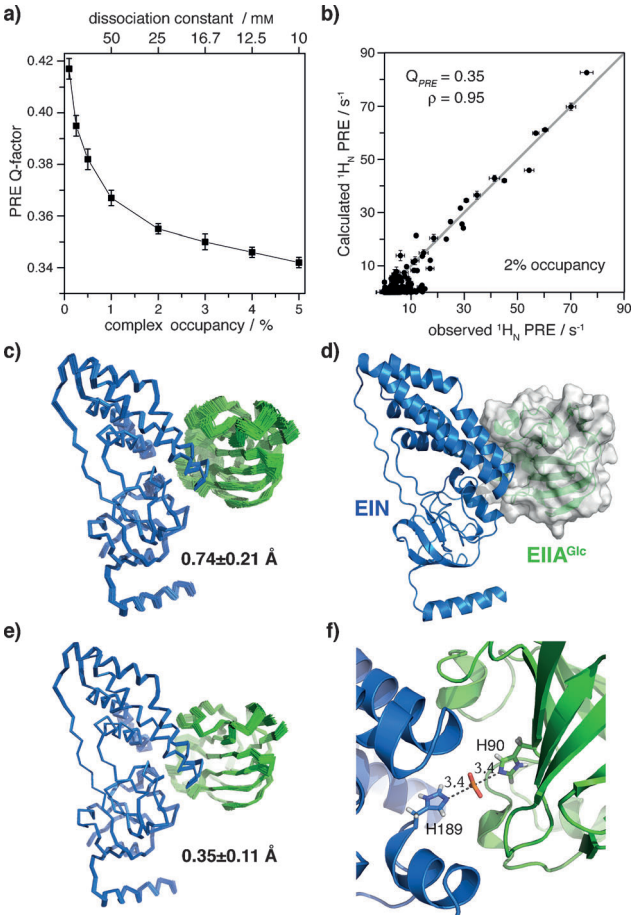

Figure 4. Structure of the EIN-EIIA^{Glc} complex. a) Overall PRE Q-factor as a function of the population of the complex. With the concentration of both proteins at 0.5 mM, a 2% occupancy corresponds to a K_D value of 25 mM (top scale). b) The PRE Q-factor and correlation coefficient ρ between observed and calculated PREs at 2% occupancy of the complex. The diagonal line indicates a perfect correlation, simply to guide the eyes. c,e) Ribbon representation for the EIN-EIIA^{Glc} complex, with backbone rms deviations indicated. Covalent geometrical restraints were incorporated when calculating the structure shown in panel (e). The ensemble was selected based on overall energy, PRE Q-factor, and deviation from the mean structure. d) Cartoon and surface representation for the complex. f) Close-up view of the complex showing the phosphorylation transition state. The distances to the phosphoryl group being transferred are labeled.

of the complex corresponds to a K_D value of about 25 mM for the EIN-EIIA^{Glc} interaction, which is within the range deduced from the CSP fitting (Figure 2d).

At 2% occupancy for the EIN-EIIA^{Glc} complex, the overall PRE Q-factor is 0.35 and the correlation coefficient is 0.95 between the observed and calculated PREs (Figure 4b). The complex structure converges to a well-defined conformation, affording root-mean-square (rms) differences of 0.74 ± 0.21 Å for the backbone and 0.99 ± 0.17 Å for all heavy atoms (Figure 4c and d). When enforcing a covalent geometry for the phosphorylation transition state, the structural convergence can be improved to 0.35 ± 0.11 Å for the backbone and 0.69 ± 0.07 Å for all heavy atoms (Figure 4e and Table S1), while the PRE Q-factor remains the same. In the transition-state complex, the distances from the phosphorus atom in the phosphoryl group to the Nε2 atoms of the active site histidines in EIN and EIIA^{Glc} are both 3.4 Å (Figure 4f), which is characteristic of a dissociative transition state for the phosphorylation reaction.[5b,13] As such, the complex structure explains how a phosphoryl group can be transferred between EI and EIIA^{Glc}. Though a well-defined complex structure is required to enable phosphoryl transfer, encounter complexes between EI and EIIA^{Glc} at even lower occupancies may exist.[14] Indeed, EIIA^{Glc} residues 38-40 and 94-97 at EIN-E63C site and EIN residues 62-71 at EIIA^{Glc}-E43C site experience PREs $> 5\ s^{-1}$ but are not fully accounted for (Figure 3).

EIN and EIIA^{Glc} are highly complementary in shape in their complex, as EIIA^{Glc} saddles over a helix of EIN (Figure 4d) and affords a total buried solvent accessible surface area of 1517 ± 128 Å^2. Over a dozen hydrophobic aliphatic and aromatic residues, including I72, L79, L115, L118, L123, and V130 in EIN and V39, V40, F41, I45, V46, F71, F88, V96 in EIIA^{Glc}, are located near the active-site residues, which would favor the formation of the complex. On the other hand, the interfaces are highly negatively charged on both EIN and EIIA^{Glc} (Figure 5a and Figure S6), which can account for the ultra-weak affinity between the two proteins.

To assess the role of charged residues at the buried interfaces, we designed a charge reversal mutant, by mutating EIIA^{Glc} residue E86 to a lysine. Titration of this E86K mutant

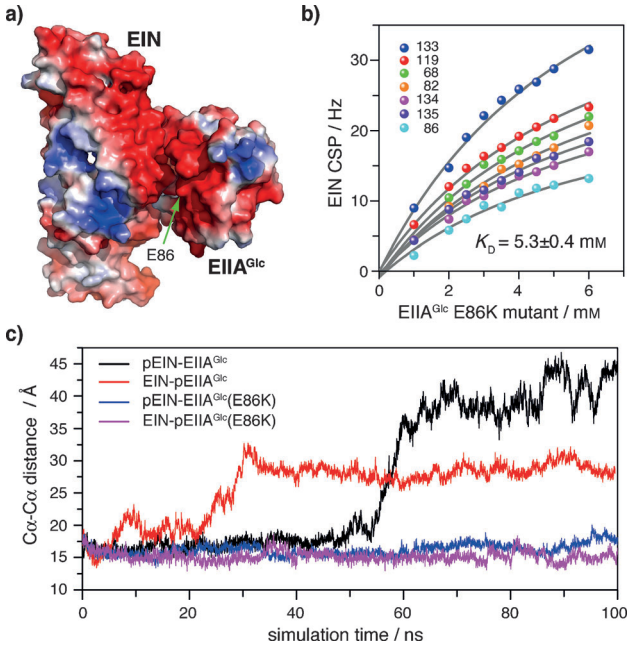

Figure 5. Physical basis for the fleeting interaction between EI and EIIA^{Glc}. a) Solvent accessible surface of EIN-EIIA^{Glc} complex colored by electrostatic potential, on a scale from −3 kT (red) to 3 kT (blue). The mutated residue in EIIA^{Glc} is denoted with a green arrow. b) Titration of EIN with EIIA^{Glc} E86K mutant protein affords CSPs that can be globally fitted to a binding isotherm. c) The distances between the Cα atoms of H189 in EIN and H90 in EIIA^{Glc} (either wild-type or E86 K mutant) during accelerated MD simulations for the fleeting complex, with the phosphoryl group attached to either EIN or EIIA^{Glc}.

of EIIA^{Glc} to EIN perturbed the same set of residues on the EIN surface as the titration with the wild-type EIIA^{Glc}, yet the magnitude of the CSPs are much larger (Figure 5b). Among the perturbed residues, residue E68 in EIN displays a 20 Hz CSP, compared to a mere 4 Hz when titrated with the wild-type EIIA^{Glc} (Figure S4). Importantly, the EIN CSPs can now be fitted to a global binding isotherm, affording a K_D value of 5.3 ± 0.4 mM (Figure 5b).

To elucidate the dynamic feature of the EIN–EIIA^{Glc} complex, we performed accelerated molecular dynamics (aMD) simulations.[15] During the phosphorylation signaling, a phosphoryl group can be either attached to EIN residue H189 or EIIA^{Glc} residue H90. The free energies calculated for these two intermediate complexes, pEIN–EIIA^{Glc} and EIN–pEIIA^{Glc}, are −9.5 and −4.3 kcal mol^{-1}, respectively. Thus, the complex is more stable with EIN phosphorylated than with EIIA^{Glc} phosphorylated. Accordingly, during the aMD simulations, the EIN–pEIIA^{Glc} complex dissociates more readily than the pEIN–EIIA^{Glc} complex does (Figure 5c). As such, the relative stabilities of these two intermediate complexes dictate that the phosphoryl signal flows from EI to EIIA^{Glc}.

Dissociation of protein–protein complexes are usually recapitulated with steered MD simulations, as the lifetime of most complexes is too long to be simulated with unbiased MD simulations.[16] The fact that the EIN–EIIA^{Glc} dissociation can be visualized with the aMD indicates that the complex is short-lived, likely on the timescale from micro- to milliseconds. Hence we term such interaction a fleeting interaction. Upon introducing an E86 K mutation to EIIA^{Glc}, the EIN–EIIA^{Glc} complex remains associated during the aMD simulations, no matter to which protein the phosphoryl group is attached (Figure 5c). As such, the charge-reversal mutation not only enhances the binding affinity, but also prolongs the lifetime of the otherwise fleeting complex.

With a K_D value of about 25 mM, the complex between EI and EIIA^{Glc} is almost an order of magnitude weaker than all known protein–protein complexes with high-resolution structures available.[4,5] So what are the advantages for such weak fleeting interaction in phosphorylation signaling? The general notion for cell signaling has been that, when stimulated, the expression level of a protein is either up-regulated or down-regulated, leading to a modulation of the corresponding signal. Here we constructed a mathematical model for an open phosphoryl transfer process within a large two-component system, and our calculation shows that higher protein concentration does lead to an amplification of phosphoryl signal (Figure 6a)—up to a 100-fold change in phosphoryl flux for every 10-fold change of protein concentration. However, the full capacity of such modulation can only be achieved when the affinity between the two interacting proteins, as measured by the K_D value, is comparable to or larger than the protein concentration (Figure 6b). If the K_D value is smaller than the protein concentration, the modulation of phosphoryl flux is relatively insensitive to the change in protein concentration.

The relationship between phosphoryl flux and K_D can also be grasped from the definition of the K_D, that is, the ratio between kinetic dissociation rate k_{off} and association rate k_{on}. A weak protein–protein interaction corresponds to a large kinetic dissociation rate k_{off} at a certain association rate k_{on}. Dissociation is intrinsic to a protein complex, whereas association can be promoted by high concentration.[17] Increasing evidences have shown that protein is unevenly distributed in cell and the local effective concentration can be well above 1 mM,[18] owing to a number of factors, such as

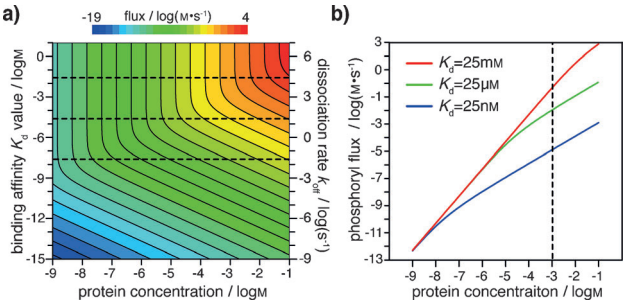

Figure 6. Phosphoryl flux as a function of the protein concentration and binding affinity K_D. a) Heat map of the phosphoryl flux from protein A to protein B at a kinetic association rate k_{on} of 10^6 M^{-1} s^{-1}. The corresponding kinetic dissociation rate k_{off} is labeled on the right, which is equal to $k_{on}K_D$. The dashed lines denote the K_D values of 25 nM, 25 μM and 25 mM, respectively. b) At these three K_D values, the phosphoryl flux as a function of protein concentration is plotted. When the protein concentration is 1 mM (denoted by a dashed line), the red flux is larger than 43 fold of the green flux, and larger than 37000 fold of the blue flux.

macromolecular crowding,[19] being part of a multi-protein complex, association with a common scaffold protein,[20] membrane anchoring,[21] and covalent linkage.[22] Thus, too strong binding at high concentration would trap the signaling proteins in a bound state, making the release of the phosphorylated product the rate-limiting step.[23]

To summarize, we have shown that phosphoryl signaling can be accomplished by an ultra-weak fleeting interaction between two bacterial enzymes. We introduced a Gd^{3+}-based probe in PRE NMR spectroscopy for the first time, and we determined the atomic resolution structure of the ultra-weak complex that is otherwise too fleeting to visualize. Though marginally stable, such a fleeting interaction would enable effective modulation of cell signal upon the changes in protein concentration. Given the millimolar effective concentrations of many proteins in cell, fleeting interactions can be prevalent among signaling proteins, which awaits further exploration.

Received: June 6, 2014
Published online: August 11, 2014

Keywords: NMR spectroscopy · paramagnetic relaxation enhancement · proteins · protein–protein interactions · signal transduction

[1] L. J. Jensen, M. Kuhn, M. Stark, S. Chaffron, C. Creevey, J. Muller, T. Doerks, P. Julien, A. Roth, M. Simonovic, P. Bork, C. von Mering, *Nucleic Acids Res.* **2009**, *37*, D412 – 416.
[2] J. R. Perkins, I. Diboun, B. H. Dessailly, J. G. Lees, C. Orengo, *Structure* **2010**, *18*, 1233 – 1243.
[3] a) I. M. Nooren, J. M. Thornton, *J. Mol. Biol.* **2003**, *325*, 991 – 1018; b) H. Hwang, T. Vreven, J. Janin, Z. Weng, *Proteins Struct. Funct. Bioinf.* **2010**, *78*, 3111 – 3114; c) P. L. Kastritis, I. H. Moal, H. Hwang, Z. Weng, P. A. Bates, A. M. Bonvin, J. Janin, *Protein Sci.* **2011**, *20*, 482 – 491.
[4] O. Vinogradova, J. Qin, *Top. Curr. Chem.* **2012**, *326*, 35 – 45.
[5] a) R. Wang, X. Fang, Y. Lu, S. Wang, *J. Med. Chem.* **2004**, *47*, 2977 – 2980; b) Y. S. Jung, M. Cai, G. M. Clore, *J. Biol. Chem.* **2012**, *287*, 23819 – 23829; c) M. A. Hass, M. Ubbink, *Curr. Opin. Struct. Biol.* **2014**, *24*, 45 – 53.
[6] T. Hunter, *Philos. Trans. R. Soc. London Ser. B* **2012**, *367*, 2513 – 2516.
[7] J. Deutscher, C. Francke, P. W. Postma, *Microbiol. Mol. Biol. Rev.* **2006**, *70*, 939 – 1031.
[8] V. Venditti, G. M. Clore, *J. Biol. Chem.* **2012**, *287*, 26989 – 26998.
[9] P. W. Postma, J. W. Lengeler, G. R. Jacobson, *Microbiol. Rev.* **1993**, *57*, 543 – 594.
[10] D. S. Garrett, Y. J. Seok, A. Peterkofsky, A. M. Gronenborn, G. M. Clore, *Nat. Struct. Biol.* **1999**, *6*, 166 – 173.
[11] G. M. Clore, J. Iwahara, *Chem. Rev.* **2009**, *109*, 4108 – 4139.
[12] I. Bertini, C. Luchinat, S. Aime, *Coord. Chem. Rev.* **1996**, *150*, 77 – 110.
[13] G. Wang, J. M. Louis, M. Sondej, Y. J. Seok, A. Peterkofsky, G. M. Clore, *EMBO J.* **2000**, *19*, 5635 – 5649.
[14] a) C. Tang, J. Iwahara, G. M. Clore, *Nature* **2006**, *444*, 383 – 386; b) A. N. Volkov, J. A. Worrall, E. Holtzmann, M. Ubbink, *Proc. Natl. Acad. Sci. USA* **2006**, *103*, 18945 – 18950; c) Y. Hiruma, M. A. Hass, Y. Kikui, W. M. Liu, B. Olmez, S. P. Skinner, A. Blok, A. Kloosterman, H. Koteishi, F. Lohr, H. Schwalbe, M. Nojiri, M. Ubbink, *J. Mol. Biol.* **2013**, *425*, 4353 – 4365.
[15] D. Hamelberg, J. Mongan, J. A. McCammon, *J. Chem. Phys.* **2004**, *120*, 11919 – 11929.
[16] R. O. Dror, R. M. Dirks, J. P. Grossman, H. Xu, D. E. Shaw, *Annu. Rev. Biophys.* **2012**, *41*, 429 – 452.
[17] X. Pang, S. Qin, H. X. Zhou, *Biophys. J.* **2011**, *101*, 1175 – 1183.
[18] J. A. Ubersax, J. E. Ferrell, Jr., *Nat. Rev. Mol. Cell Biol.* **2007**, *8*, 530 – 541.
[19] a) H. X. Zhou, G. Rivas, A. P. Minton, *Annu. Rev. Biophys.* **2008**, *37*, 375 – 397; b) B. Akabayov, S. R. Akabayov, S. J. Lee, G. Wagner, C. C. Richardson, *Nat. Commun.* **2013**, *4*, 1615.
[20] T. J. Gibson, *Trends Biochem. Sci.* **2009**, *34*, 471 – 482.
[21] X. Shi, Y. Bi, W. Yang, X. Guo, Y. Jiang, C. Wan, L. Li, Y. Bai, J. Guo, Y. Wang, X. Chen, B. Wu, H. Sun, W. Liu, J. Wang, C. Xu, *Nature* **2013**, *493*, 111 – 115.
[22] J. Y. Suh, J. Iwahara, G. M. Clore, *Proc. Natl. Acad. Sci. USA* **2007**, *104*, 3153 – 3158.
[23] S. A. Lieser, B. E. Aubol, L. Wong, P. A. Jennings, J. A. Adams, *Biochim. Biophys. Acta Proteins Proteomics* **2005**, *1754*, 191 – 199.

